AUTOMATIC DETECTION OF CALCIFIED LESIONS IN THE DESCENDING AORTA USING CONTRAST ENHANCED CT SCANS

R. Shahzad [1,2], *M. Schaap* [1], *F. B. Goncalves* [3], *C. T. Metz* [1], *H. Tang* [1,2]
T. van Walsum [1], *A. Moelker* [3], *L. J. van Vliet* [2], *W. J. Niessen* [1,2]

[1] Biomedical Imaging Group Rotterdam, Dept. of Radiology and Medical Informatics, Erasmus MC, Rotterdam,The Netherlands
[2] Quantitative Imaging Group, Imaging Science and Technology, Faculty of Applied Science, Delft University of Technology, Delft, The Netherlands
[3] Dept. of Radiology, Erasmus MC, Rotterdam, The Netherlands

ABSTRACT

In clinical practice, detection and quantification of calcified lesions in the coronary arteries and aorta is normally performed on non contrast enhanced Computed Tomography (CT) scans. This CT scan is generally followed by a contrast enhanced angiography (CTA) scan for better plaque visualization. We propose and evaluate a method for the detection of calcified lesions on CTA scans. Calcium lesion detection is straightforward on a CT scan, however performing the same task on a contrast enhanced angiography (CTA) scan is challenging, as the intensity of the contrast enhanced vessel lumen is very similar to that of calcium. Our method is based on semi-automatic centreline extraction and subsequent segmentation of high intensity objects to detect calcified lesions in the descending aorta. The method is evaluated on 19 datasets, and the results are compared to manual detection of calcifications on the CT scan. The proposed method has an accuracy of 82.4%, and 91% of the calcified lesions were successfully detected on the CTA scans.

***Index Terms*—** CT, CTA, Aorta, Calcified plaque, calcium detection.

1. INTRODUCTION

Several studies have shown the relation between vascular calcifications and the risk of future health complications. The presence of calcified lesions in the coronary arteries is a biomarker for coronary artery disease (CAD). Calcifications in the aorta and iliac arteries have been associated with hypertension, diabetes, renal failure as well as cardiovascular events [1], [2], [3]. In order to further support these investigations, large clinical and epidemiological studies are needed which require techniques to automatically and accurately quantify calcifications.

In clinical practice detection and quantification of calcified lesions is performed on non-enhanced CT scans. Generally, a CT scan is followed by a CTA scan, in which the presence of intra venous (IV) contrast agent helps to better assess the vessel lumen (stenosis) and vessel wall [4]. The CTA protocol, yields images with less noise and higher resolution for better visualization. Detection and quantification of calcifications in CTA scans would allow an imaging protocol without a CT scan, thus reducing scanning time and radiation dose. Furthermore, additional information on the vessel lumen in CTA images may aid in the detection of calcifications, although the distinction between lumen and calcium is hampered by the increased lumen intensity.

The purpose of our study is to develop and evaluate an algorithm to detect calcium lesions directly on the CTA scans. The performance of the method is evaluated quantitatively by comparing the lesions detected by the algorithm in nineteen abdominal CTA scans with those manually annotated in corresponding CT scan (gold standard).

2. METHOD

The method consists of four stages, a semi-automatic vessel centreline extraction step (user defines the start and the end of the aorta), followed by segmentation of the high intensity objects, feature extraction of candidate objects, and finally classification step. Each of these steps are explained in the sub sections below.

2.1. Centreline Extraction

We adapted an iterative two point minimum cost path centreline extraction method for obtaining the centrelines in the aorta. Basically the method finds the 3D path of least cost between two manually placed seed points [5].

An initial centreline is obtained by using a multi-scale vesselness filter [6]. The cost image used for the centreline

extraction is defined as:

$$C_v = \frac{1}{(V_o + \epsilon)} \tag{1}$$

where V_0 is the multi-scale vesselness measure and ϵ is a small positive value introduced to avoid singularities.

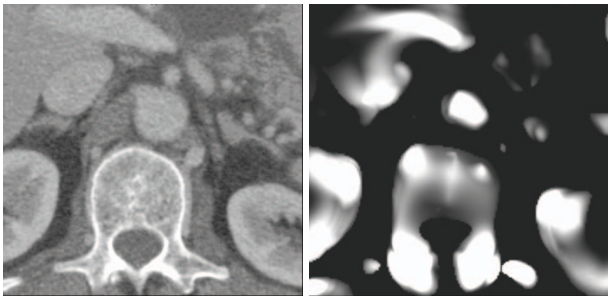


Fig. 1. An axial slice from one of the CTA scans and the corresponding vesselness image

Subsequently, we generate a stack of multi-planar reformatted (MPR) images perpendicular to the initial centreline, and iteratively apply a minimum cost path approach to this stack of images, using a modified cost image (similar to Tang et al. [7]). The cost image used for this step is defined as:

$$C_m = \frac{1}{(M + \epsilon)} \tag{2}$$

where M is a medialness measure [8] and ϵ is a small positive value to avoid singularities. The cost image generated from Eq(2) is then used to extract the refined centreline. One iteration proved to be sufficient for our purpose.

We use the medialness feature in the centreline refinement phase, as it has better centralizing properties than the vesselness feature.

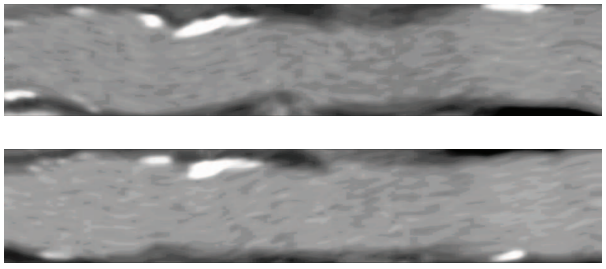


Fig. 2. CMPR images having a FOV of 30 mm constructed using the initial centrelines (top) and the corrected centrelines after using Eq(2) (below), it can be appreciated that the vessel wall is much more parallel.

2.2. Segmentation of the high intensity objects

To obtain a well defined region for selecting the candidate objects a segmentation approach was used. The segmentation is performed on the MPR image stack of the aorta which was obtained using the extracted centreline. The segmentation makes use of lumen intensity similarity to separate the contrast agent in the lumen from the calcium and the surrounding tissue.

We calculate the likelihood of a voxel belonging to the contrast within the lumen based on the differences between the intensity of the voxel and an estimate of the lumen intensity (obtained using the centreline), and the estimate of difference between the lumen and surrounding tissue [9]:

$$Pr(I_x|f_x = 1) = -0.5\left(0.75 - 0.25erf\left(\frac{D_x - T_{in}}{\sigma_i}\right)\right) \left(erf\left(\frac{D_x - T_{out}}{\sigma_i}\right) - 1\right) \tag{3}$$

with $D_x = |I_x - \hat{I}_{\acute{x}}|$ the absolute difference between the intensity of the voxel and the local intensity estimate. T_{in} is the threshold parameter within the lumen, T_{out} = λ(Mean(I) - I_o) which defines the threshold parameter outside the lumen [9]. Fig. 4(b) shows the result of the segmentation step. All the voxels which have an intensity similar to the contrast agent appear bright whereas the surrounding tissue and calcium dark.

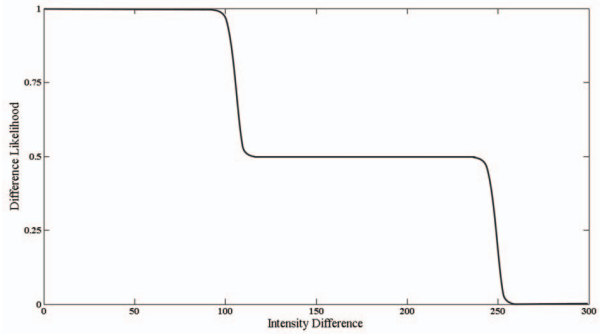


Fig. 3. $Pr(I_x|f_x = 1)$ with $T_{in} = 100$ and $T_{out} = 250$

2.3. Candidate feature extraction

Although the segmentation step clearly masks out all the voxels that have intensities different to that of the lumen (calcification and surrounding tissue) it sometimes also detects parts of the spine due its close vicinity. We use a classification step to detect the true calcium objects. First we obtain the candidate objects by thresholding the MPR image stacks (as shown in Fig. 4 (c)) that were masked by the segmentation and extract the connected-components using an 18-neighbourhood relationship to obtain the objects. Any object less than 3 voxels in size is considered as image noise and discarded. To be able to differentiate the spine objects from the true calcium objects we constructed a classifier based on the following features: volume, maximum intensity,

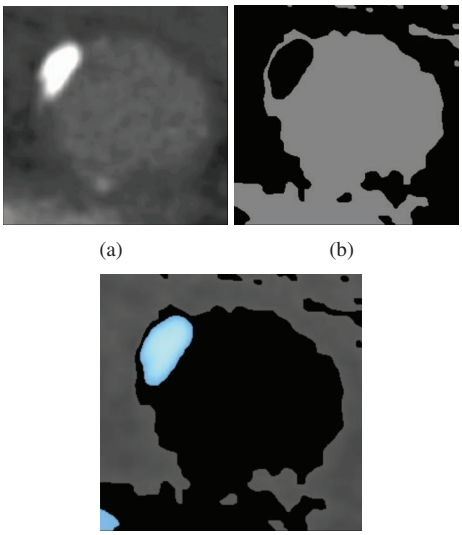


Fig. 4. A MPR stack image (a), corresponding segmented image (b), the candidate objects selected in blue (c)

average intensity, blob likeness, plate likeness and distance to the centreline for each of the detected object. Blob likeness is defined as $B = \frac{|\lambda_1|}{\sqrt{|\lambda_2\lambda_3|}}$ and plate likeness is defined as $P = \frac{|\lambda_2|}{|\lambda_3|}$, where $|\lambda_1| \leq |\lambda_2| \leq |\lambda_3|$ are the eigenvalues of the central image moments of the candidate object.

2.4. Classifier selection and training

We trained a classifier to be able to differentiate the true aortic calcifications from the false objects (parts of the spine and some image noise). We randomly divided our data set into training and testing sets. We tested 4 different classifiers: linear discriminate classifier (LDC), quadratic discriminate classifier (QDC), Parzen classifier, and K-nearest neighbour classifier (K-NN).

3. EXPERIMENTS

3.1. Data acquisition and object labelling

We retrospectively obtained 19 datasets of subjects for which both the CT and CTA scans were available. These datasets were acquired at the Erasmus MC, Rotterdam, The Netherlands. Both scans were acquired on the same day and using the same scanner (Siemens Medical Solutions, Forchheim, Germany). However due to the different CT and CTA protocols, the image data have different resolutions. The CT scans have between 40 to 223 slices in the z direction and an in-plane voxel size of 0.85 x 0.85 mm^2 on average and a slice thickness of 5 mm and were reconstructed using a b30f (medium to smooth) convolution kernel. The CTA scans have between 40 to 234 slices in the z direction and an in-plane voxel size of 0.84 x 0.84 mm^2 on average and a slice thickness between 3 and 5 mm and were also reconstructed using a b30f (medium to smooth) convolution kernel. Both scan types were reconstructed to a matrix size of 512 x 512.

The CT scans are used to obtain the ground truth for calcium object detection. In order to compute the correspondence between the objects in the CT and CTA scans a multi-stage image registration was used. Initially a multi-resolution coarse to-fine affine registration was performed in three steps. For each resolution level we applied 256 iterations of a stochastic gradient descent optimizer. As a cost function, the mean square difference (MSD) was used. The results of the affine registrations were used to initialize a non-rigid (B-splines) registration, using mutual-information as a similarity measure. For each resolution 1024 iterations of a stochastic gradient descent optimizer were applied. A B-spline grid was defined by control points with 20mm separation. Elastix, a publicly available medical image registration software package was used [10]. The results of the registration step were visually inspected to check for accuracy.

The detected candidate objects from the training CTA scans were labelled as positive objects or negative objects using the CT-CTA registration information.

3.2. Parameters

For the vesselness measure the lower and upper scales for the filter were set to 5 mm and 10 mm. For the medialness measure the minimum and maximum scales were set to 5 mm and 25 mm and the number of intermediate steps to 100. The value of ϵ used to generate the cost images was set to 0.0001. The MPR images were generated at 1 mm distance perpendicular to the centreline having a cross-sectional region of 30 mm, and corresponding to a voxel size of 0.1 x 0.1 x 1 mm^3. The parameters for the segmentation step were set to σ_i = 5, $I_o = 1100$, $\lambda = 0.75$ and $T_{in} = 100$. The value of the threshold parameter for performing the connected component analysis for object detection was image dependent and was set to the mean intensity value of a 6 x 6 x 3 voxel neighbourhood around the second seed point. The classifier was trained on nine datasets and tested on nine other datasets. From the pilot experiments performed on the training set, a 3-NN classifier gave the best results with respect to the classification error. One dataset had to be excluded because it had a large aneurysm and the method failed.

3.3. Object Evaluation

We performed two evaluations: first we evaluate whether all the candidate objects are picked up after the segmentation stage on the entire dataset (training+testing) and second we

determine the accuracy of the classification step (on the testing dataset). The CT-CTA registration information was used to obtain the correspondence between the objects.

3.3.1. Evaluation of candidate detection

We compared the results obtained after candidate detection on all 18 scans. Out of 342 true aortic calcifications six objects were missing after the segmentation step on the CTA scan. This corresponds to 0.32 errors/scan at the first level, the average volume of the object being left out was estimated to be 30.73 mm^3 on the CT scan and no more than 2 objects were missed per scan.

3.3.2. Evaluation of classification

The 3-NN classifier was trained on nine randomly selected datasets. The training set had a total of 276 candidate objects out of which 202 were true calcium lesions. The trained classifier was tested on nine other datasets, which contained a total of 173 candidate objects. The system has an accuracy of 82.4% while making 2.1 false positive errors/scan. The system correctly classifies 91% of the true positive objects.

Table 1. Classification results on the Test Set

	Estimated Labels		
	N	**P**	Total
True **N**	20	19	39
Labels **P**	12	122	134
	32	141	

4. DISCUSSION AND CONCLUSION

A method for automatic detection of calcium lesions in CTA is proposed. The results show that this framework yields a sensitivity of 91%. We used a two stage centreline extraction step to obtain an optimal centreline that helps improve further processing (segmentation and the distance to the centreline feature). We also observed that the six objects which were missing after the segmentation step had a very similar intensity to that of the contrast agent implying that they were low density objects.

A drawback of the method is the detection of false positive objects mostly from the spine. For future work we propose to use an atlas-based segmentation step to mask out the spine from the scan, thus reducing the number of false objects drastically. We also plan to quantify the calcium objects detected. However detection of the objects is the initial step before quantification and the framework mentioned in this paper is quite robust in detecting the calcified lesions. The current framework can also be easily adapted for detecting calcifications in the iliac arteries.

5. REFERENCES

[1] J.A. Davila, C.D. Johnson, T.R. Behrenbeck, T.L. Hoskin, and W.S. Harmsen, "Assessment of cardiovascular risk status at ct colonography," *Radiology*, vol. 240, no. 1, pp. 110, 2006.

[2] J. Takasu, R. Katz, K. Nasir, J.J. Carr, N. Wong, R. Detrano, and M.J. Budoff, "Relationships of thoracic aortic wall calcification to cardiovascular risk factors: the multi-ethnic study of atherosclerosis (mesa)," *American Heart Journal*, vol. 155, no. 4, pp. 765–771, 2008.

[3] "Cardiovascular diseases, fact sheet 317.," World Health Organization,, 2011.

[4] G.D. Rubin, "Ct angiography of the thoracic aorta," in *Seminars in Roentgenology*. Elsevier, 2003, vol. 38, pp. 115–134.

[5] C.T. Metz, M. Schaap, A.C. Weustink, N.R.A. Mollet, T. van Walsum, and W.J. Niessen, "Coronary centerline extraction from ct coronary angiography images using a minimum cost path approach," *Medical Physics*, vol. 36, no. 12, pp. 5568–5579, 2009.

[6] A. Frangi, W. Niessen, K. Vincken, and M. Viergever, "Multiscale vessel enhancement filtering," *Medical Image Computing and Computer-Assisted Interventation-MICCAI*, pp. 130–137, 1998.

[7] H. Tang, T. van Walsum, R. van Onkelen, R. Hameeteman, S. Klein, M. Schaap, F. L. Tori, Q. J. A. van den Bouwhuijsen, J. Witteman, A. van der Lugt, L. van Vliet, and W. J. Niessen, "Semiautomatic carotid lumen segmentation for quantification of lumen geometry in multispectral mri," *Submitted to Medical Image Analysis*.

[8] M. Akif Gülsün and Hüseyin Tek, "Robust vessel tree modeling," in *Medical Image Computing and Computer-Assisted Interventation-MICCAI*. 2008, pp. 602–611, Springer-Verlag.

[9] M. Schaap, L. Neefjes, C. Metz, A. van der Giessen, A. Weustink, N. Mollet, J. Wentzel, T. van Walsum, and W. Niessen, "Coronary lumen segmentation using graph cuts and robust kernel regression," in *Information Processing in Medical Imaging*. Springer, 2009, pp. 528–539.

[10] S. Klein, M. Staring, K. Murphy, M.A. Viergever, and J. Pluim, "Elastix: a toolbox for intensity-based medical image registration," *Medical Imaging, IEEE Transactions on*, vol. 29, no. 1, pp. 196–205, 2010.